Mechanistic Links Between Climatic Forcing and Model-based Plankton Dynamics in the Strait of Georgia, Canada

Karyn D. Suchy[1], Susan E. Allen[1], and Elise Olson[2]

[1]Department of Earth, Ocean and Atmospheric Sciences, University of British Columbia, Vancouver, BC, Canada. [2]Atmospheric and Ocean Sciences, Princeton University, Princeton, NJ, USA.

Corresponding author: Karyn Suchy (ksuchy@eoas.ubc.ca)

Key Points:

- Spring diatom biomass peak shifted earlier and summer diatom biomass was lower during warm years.
- Zooplankton grazed on a higher proportion of nanoflagellates during summers with weak winds.
- Winds during the summer had the strongest influence on nutrient resupply to the surface layers and to the food available to zooplankton.

Abstract

Large scale climate indices such as the North Pacific Gyre Oscillation (NPGO) have been linked to variability in both phytoplankton and zooplankton, yet the mechanisms by which they are linked remain unknown. We used a three-dimensional coupled biophysical model, SalishSeaCast, to determine the mechanistic links between the NPGO and plankton dynamics in the Strait of Georgia, Canada. First, we compared bottom-up processes during NPGO positive (cold-phase) and negative (warm-phase) years. Then, we conducted a series of model experiments to determine the effects of the NPGO on local physical drivers by switching individual parameters between a typical warm and cold year. The model showed that higher SST and weaker winds contributed to an earlier increase in spring diatom biomass during warm-phase years. Due to the conditions set up during the spring, warm-phase years exhibited lower overall summer diatom biomass and an earlier shift to nanoflagellate-dominance compared to cold-phase years. Our systematic model experiments revealed that variability in wind-driven resupply of nutrients to the surface waters during the summer had the most significant impact on diatom biomass, and ultimately on the food available to zooplankton grazers. The Z1 and Z2 model classes grazed on a higher proportion of nanoflagellates during the summer of warm-phase years, suggestive of a poorer quality diet consumed during warm years. Results from this study are relevant in the context of other climate signals (e.g., El Niño) favouring weaker winds or increased stratification, which would limit the amount of nutrients being replenished to the surface waters.

Plain Language Summary

The North Pacific Gyre Oscillation with cold- and warm-phases is an example of a climate pattern that has previously been linked to changes in phytoplankton and zooplankton in the Strait of Georgia, Canada. We used a three-dimensional physical and biological model of the Salish Sea to determine the ocean processes linking large-scale climate patterns to variations in plankton. Physical, chemical, and biological parameters were compared between cold-phase and warm-phase years. Then, we ran a series of model experiments to determine which parameter(s) had the strongest influence on the plankton. The model showed that diatoms (larger phytoplankton) peaked earlier during warm years, but had lower overall summer biomass. As a result, zooplankton fed mainly on nanoflagellates (smaller phytoplankton) during warm years. Our experiments showed that summer winds had the strongest influence on nutrient resupply to the surface waters for diatom growth and, ultimately, the food available to zooplankton. These results suggest that zooplankton may feed on a poorer quality diet during warm years, which is relevant in the context of numerous climate signals and future warming scenarios.

1 Introduction

Interannual variations in phytoplankton dynamics, including spring bloom timing, standing stock biomass, and shifts in community composition, have a direct impact on the quantity and quality of food available to zooplankton grazers in marine ecosystems. In turn, the integrated effects of this variability in phytoplankton dynamics on zooplankton biomass determines the amount of energy transferred to higher trophic levels. Over longer time scales, it is critical to understand the mechanistic links between this interannual variability in lower trophic levels (phytoplankton and zooplankton) and large-scale climate indices, which often

drives local variations in environmental parameters at either regional or basin-wide levels over decadal timescales.

One example of a large-scale climate pattern is the North Pacific Gyre Oscillation (NPGO), which emerges as the second dominant mode of variability in sea surface height (SSH) in the Northeast Pacific (Di Lorenzo et al., 2008). The NPGO mode closely tracks the second EOF of North Pacific SST anomalies, also known as the "Victoria Mode" (Bond et al., 2003). In addition, the NPGO is strongly correlated with previously unexplained fluctuations in surface layer salinity, nutrient, and chlorophyll *a* concentrations in both the Gulf of Alaska and the California Current (Di Lorenzo et al., 2008). Fluctuations in the NPGO are correlated with regional and basin-scale variations in wind-driven upwelling and horizontal advection – the fundamental processes controlling salinity and nutrient concentrations, which drive changes in phytoplankton concentrations and potentially throughout the food web.

Previous studies have linked NPGO to variability in both phytoplankton and zooplankton. For example, in the California Current System (CCS), shifts in phytoplankton community composition coincided with major phase shifts of both the NPGO and the Pacific Decadal Oscillation (PDO), with warm-phase (i.e., NPGO negative) years having a higher proportion of dinoflagellates compared to diatoms (Barth et al., 2020). Spring phytoplankton bloom timing has also been significantly correlated with a positive NPGO on the Alaskan Shelf resulting in a later diatom peak during cold years (Batten et al., 2018). In addition, numerous studies have examined the lagged effects of NPGO on zooplankton communities. Positive phases of the NPGO (cold years) lagged by 3-4 years coincided with higher-than-average mesozooplankton biomass in the North Pacific Subtropical Gyre at station ALOHA (A Long-term Oligotrophic Habitat Assessment; Valencia et al., 2016). Furthermore, decadal-scale zooplankton biogeography in the

Kuroshio-Oyashio Extension (KOE) region was influenced by the NPGO when lagged by 2.5 years via changes in the advection transport of zooplankton (Chiba et al., 2013).

The Strait of Georgia (SoG) is a semi-enclosed region between Vancouver Island and mainland British Columbia within a larger coastal water body known as the Salish Sea (Fig. 1). The SoG is an important habitat for migratory and resident fish species such as Pacific Salmon and Pacific Herring, which feed on zooplankton. Linkages between zooplankton and large-scale climate indices within the Strait of Georgia (SoG), Canada, are complex, with results varying depending on the timescales of the studies, as well as whether community composition or overall biomass is considered. Zooplankton community composition within the surface 20 m has been linked to the Southern Oscillation Index (SOI) in the SoG (Li et al., 2013). Furthermore, Suchy et al. (2022) determined that SOI was related to crustacean community composition whereas the NPGO was linked to SST and spring chlorophyll *a* bloom initiation. In terms of overall biomass, Mackas et al. (2013) examined zooplankton biomass anomalies in the SoG from 1990-2010 and found a significant positive correlation with NPGO (Fig. 2). Similarly, an examination by Perry et al. (2021) of zooplankton biomass anomalies from 1996-2018 (a portion of the same dataset analyzed by Mackas et al., 2013) determined that the PDO was a significant driver of zooplankton biomass variability (Fig. 2). Although these studies delineate two different large-scale climate indices as the drivers of zooplankton biomass in the region, they do not necessarily disagree as the NPGO and PDO were highly correlated during the time period examined (Litzow et al., 2020; Perry et al., 2021).

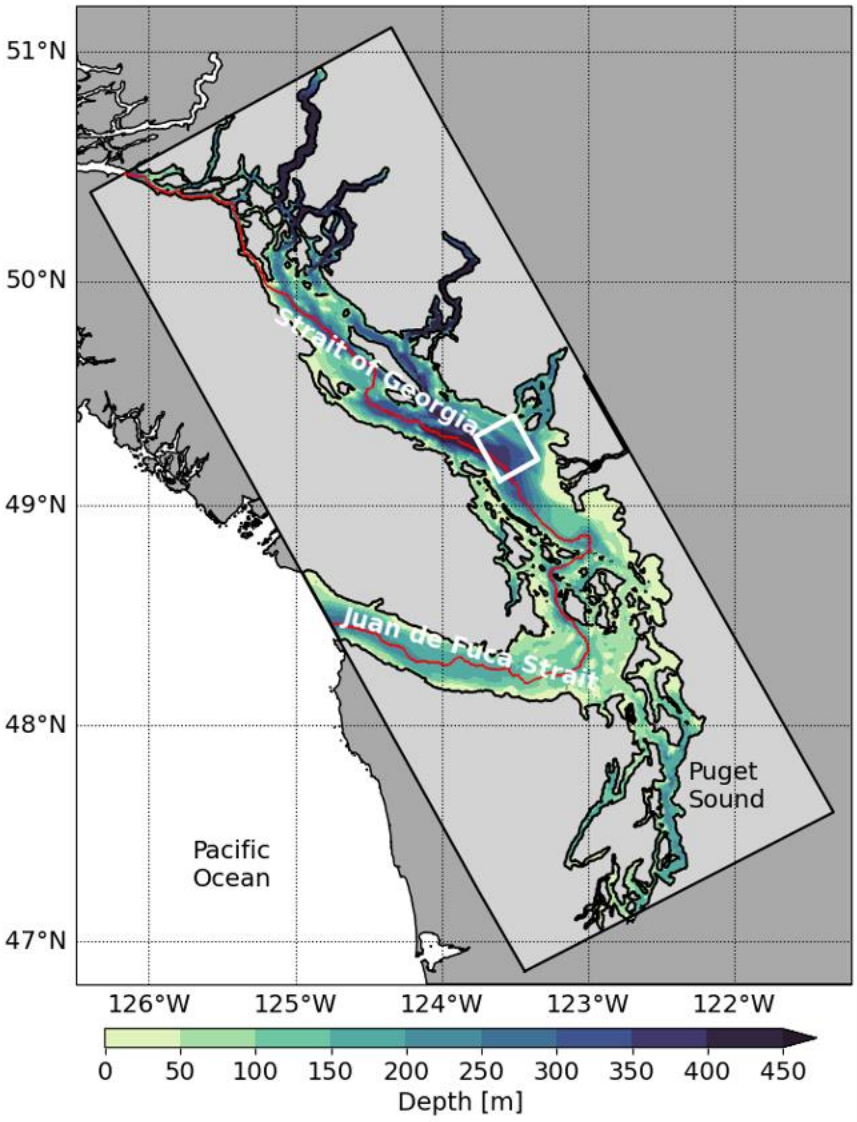

Figure 1. Map showing the study region, Central Strait of Georgia, BC, indicated with a white box. Model domain is the area within the light grey box. The thalweg, the deepest connecting passage, is indicated in red.

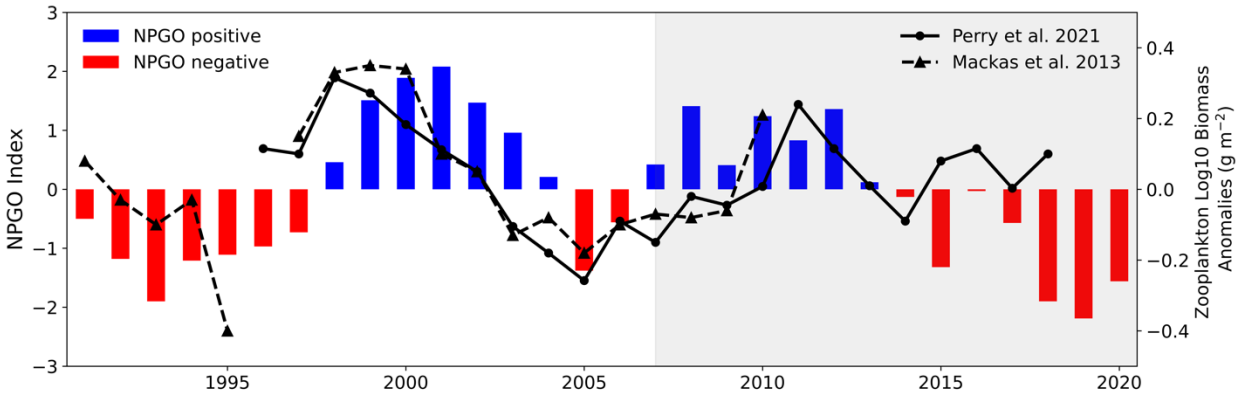

Figure 2. NPGO index from 1991 to 2020 vs zooplankton biomass anomalies extracted from Mackas et al., (2013) and Perry et al., (2021). SalishSeaCast model years (2007 to 2020) are shaded in grey.

While these studies have previously linked warm-phase conditions to changes in phytoplankton bloom timing and zooplankton biomass and community composition, the exact mechanisms by which large-scale climate indices impact food web dynamics, including higher trophic levels, remains unknown (Hertz et al., 2016; Hipfner et al., 2020). This gap in knowledge is due, in part, to the lack of simultaneous measurements of physical conditions, nutrients, phytoplankton and zooplankton (and higher trophic levels) across the same timescales. In addition, temporal autocorrelations between many of the environmental and physical variables, as well as the longer time scales necessary to resolve decadal-scale oscillations, often complicate statistical analyses.

Here, we used a three-dimensional coupled biophysical model, SalishSeaCast, to examine how the NPGO is linked to local physical drivers and, ultimately, to phytoplankton and the resulting food available for zooplankton. We used a 14-year (2007-2020) time series of model output to compare bottom-up processes in cool versus warm years in the Central SoG, Canada (Fig. 1). This time period in the Salish Sea was characterized by an NPGO positive (cold) period

prior to 2014 and an NPGO negative (warm) period from 2014 on, local impacts of the North Pacific marine heatwave (primarily on 2015-2016; Bond et al., 2015), and long-term warming. We focused our analysis on the four strongest positive (cold) and negative (warm) NPGO years. In addition, we used the model to examine the effects of the NPGO on specific local physical drivers within the Central SoG using a series of experiments wherein we swapped individual physical parameters between a "typical" warm and a "typical" cold year. Results from these experiments allowed us to delineate the specific physical parameters responsible for any significant changes in the phytoplankton community and zooplankton grazing within the region. While we focused on the NPGO due to its known association with observation data, we show that this signal is also evident in the model. Furthermore, because our goal was to determine mechanistic links, we go beyond the NPGO to other climate signals in our interpretation of the results.

2 Methods

2.1 Study Region

The Strait of Georgia (SoG) has a surface area of approximately 6515 km^2 with a maximum depth of over 400 m (Thomson, 1981) and is connected to open ocean waters at both its northern and southern ends. The main source of freshwater into the strait is the Fraser River, which plays an important role in stratification that varies with the seasonal influence of river input (Harrison et al., 1983). This influx of freshwater results in an estuarine-like circulation with surface waters (mostly) leaving the SoG via the Juan de Fuca Strait to the south and deeper, nutrient-rich water being upwelled into the surface (Li et al., 2000; Pawlowicz et al., 2007). Our study focused on the Central SoG (white box; Fig. 1), as historical zooplankton sampling was

most comprehensive in this region. Phytoplankton biomass in the Central SoG typically peaks in March (Peña et al., 2016), but bloom timing varies between February to early April (Allen & Wolfe, 2013; Suchy et al., 2022), whereas zooplankton biomass peaks in late-spring or late-summer (Mackas et al., 2013). In addition, the Central SoG is one of the main regions associated with migrating juvenile salmon species (Beamish et al., 2012; Furey et al., 2015), with Coho and Chinook salmon typically entering the strait in mid- May (Beamish et al., 2010; Neville et al., 2015).

2.2 Study Period

Our model study period was from 2007 to 2020 (Fig. 2), which is a relatively short time series compared to the timescale (decades) of NPGO variability. Monthly NPGO Index data were downloaded (http://www.o3d.org/npgo/npgo.php) and subsequently used to calculate annual anomalies. Annual NPGO Index values during some of the years in our time series were neutral or close to neutral. As such, we selected the four years with the strongest negative NPGO Index (2008, 2010, 2011, and 2012; “cold-phase years”) and the four years with the strongest positive NPGO Index (2015, 2018, 2019, and 2020; “warm-phase years”) for our analyses. We note that there were other confounding signals in the region throughout this time. Notably, the Northeast Pacific marine heatwave was an anomalously warm water event that formed during winter 2013/2014 (Bond et al., 2015), persisting through to 2017. In addition, operating on shorter time scales are the El Niño and La Niña events, which result in variations in local environmental drivers (e.g., Fraser River flow) in the region (Suchy et al., 2019). Although our study is motivated by the previously identified association between NPGO and zooplankton variability, the model employed is a realistic 14-year simulation including the effects of multiple

184 climatic drivers. Thus, the interannual patterns in bottom-up forcing identified herein occurred in
185 response to combined climatic forcings over the modelled time period.
186
187 2.3 SalishSeaCast Model
188 The SalishSeaCast model domain covers the entire Salish Sea (Fig. 1) with a horizontal
189 resolution of approximately 500 m and a vertical resolution ranging from 1 at the surface to 27 m
190 at the bottom. The physical component of SalishSeaCast is an implementation of Nucleus for
191 European Modelling of the Ocean (NEMO Version 3.6; Madec et al., 2017) and is described in
192 detail in Soontiens et al., (2016) and Soontiens & Allen, (2017) with subsequent relevant
193 changes outlined in Olson et al., (2020) and Jarníková et al., (2022). The model is forced with a
194 monthly climatology of over 150 rivers in the region (Morrison et al., 2012). Atmospheric
195 forcing (winds, solar radiation) is derived from High Resolution Deterministic Prediction System
196 (HRDPS) atmospheric model output (Milbrandt et al., 2016). SalishSeaCast has two open
197 boundaries for temperature, salinity, and nutrients: one at Johnstone Strait and one at the mouth
198 of the Strait of Juan de Fuca. Prior to 2013, boundary conditions were based on fields from NEP
199 3.6 (Lu et al., 2017). After 2013, open boundary conditions were based on fields from the
200 LiveOcean model (Davis et al., 2014; Siedlecki et al., 2015).
201 The biological component of the model, SMELT (Salish Sea Model Ecosystem-Lower
202 Trophic), follows the transfer of the model's currency (nitrogen) between nutrients, primary
203 producers, grazers, and detrital pools with coupled silicon cycling. The nutrients in the model are
204 nitrate, ammonium, and dissolved silica. There are three groups of primary producers including
205 diatoms, nanoflagellates, and the mixotrophic ciliate *Mesodinium rubrum*. *M. rubrum* is included
206 as a separate class because this species periodically dominates the photosynthetic biomass in this

region (Harrison et al., 1983; Pawlowicz et al., 2007), but it forms a small portion of the overall model phytoplankton. Diatoms in the model have the highest maximum growth rates, the highest optimal light levels, and are the only class to take up silicon (Olson et al., 2020). As such, they are considered opportunists in the model (see Jarníková et al., 2022), whereas nanoflagellates, or the gleaners in the model, have the lowest maximum growth rate but compete better at low nitrogen concentrations and high temperatures (Olson et al., 2020; Jarníková et al., 2022). We provide an evaluation of the model diatom and nanoflagellate classes against high performance liquid chromatography (HPLC) data from the Canadian waters of the Salish Sea (Nemcek et al., 2023) in Supp. Fig. S1. Briefly, the evaluation showed that larger, centric diatoms (Diatoms-1 in Nemcek et al., 2023) are well represented by the model diatom class, whereas the model nanoflagellate class showed the strongest relationships with cryptophytes, prasinophytes, and haptophytes (Supp. Fig. S1). The temperature response for each phytoplankton group is set so that the optimal temperature for growth for diatoms (12ºC) and nanoflagellates (18ºC) match those of diatoms and dinoflagellates in Khangaonkar et al., (2012) after experiments with these settings showed improved summer chlorophyll bias. Diatoms become nitrate-limited at 2.0 µM N, whereas the half-saturation constant prescribed for flagellates is 0.1 µm N (Olson et al., 2020). Additionally, the model includes biogenic silica, detrital particulate organic nitrogen (PON), and dissolved organic nitrogen (DON).

Heterotrophs in SalishSeaCast are represented by two zooplankton classes: Z1 and Z2. Minor adjustments in biological tuning since Olson et al., (2020) are outlined in Jarníková et al., (2022), and those affecting zooplankton rates are provided in Suchy et al., (2023). Details of each zooplankton class, including evaluations of Z1 and Z2 against observation data, are also provided in Suchy et al., (2023). The Z1 class freely evolves based on model dynamics (Olson et

al., 2020) and represents a catch-all for taxa whose growth rates respond quickly to local conditions (Suchy et al., 2023). Z2 are the highest trophic level whose grazing impact is included in the model. While the domain-mean Z2 biomass is constrained to an annual cycle, the Z2 biomass is distributed spatially throughout the model domain in proportion to food availability. Thus, variability in the spatial distribution of Z2 throughout the domain will directly reflect interannual differences in the spatial distribution of the classes that make up its food. Assuming the concentrations of all prey items are equal, Z1 preferentially feed on flagellates and diatoms (30 and 26% of total grazing, respectively) whereas the Z2 class preferentially feeds on diatoms and Z1 (29% for each class; Suchy et al., 2023). However, the actual proportion of grazing on each class is a function of both preference and the relative abundance of the various classes. This study is based on v201905 of SalishSeaCast.

2.4 Physical and Chemical Data

We analyzed 14 years (2007-2020) of monthly model output from SalishSeaCast. Model data from the Central SoG study area were averaged over the four strongest NPGO negative and the four strongest NPGO positive years to compare each environmental parameter between cold-phase and warm-phase years. Surface (0.5 m) values were extracted for Conservative Temperature (Θ; hereafter referred to as SST), Absolute Salinity (S_A; hereafter referred to as SSS), and photosynthetically active radiation (PAR). Conservative Temperature and Absolute Salinity were used according to the Thermodynamic Equation of Seawater – 10 (TEOS-10) international standards for calculating thermodynamic properties in ocean models (IOC; SCOR & IAPSO, 2010). Halocline strength, a proxy for water column stratification, was calculated as the difference in salinity divided by the difference in depth of the two model grid cells wherein

253 the maximum salinity gradient was observed. Hourly wind data from HRDPS were interpolated
254 onto the model grid and then calculated as mean monthly wind speed values. Daily Fraser River
255 discharge data from 2007-2020 were obtained from Environment and Climate Change Canada
256 (www.wsc.ec.gc.ca/applications/H20/index-eng.cfm) from Station 08MF005 at Hope, BC.
257 Model output for nitrate and silicon were depth-averaged over the 0-10 m depth range to
258 approximate nutrient concentrations over the upper euphotic zone. Environmental data and
259 nutrients are presented as monthly seasonal cycles and as mean seasonal values over spring
260 (March to May) and summer (June to August).
261
262 2.5 Biological Data
263 Model output for phytoplankton (diatoms and nanoflagellates) biomass were depth-
264 integrated over the 0-100 m depth range and averaged over the seasonal cycles of cold versus
265 warm years. In addition, thalweg plots were used to compare the temperature dependence, as
266 well as the light and nutrient limitation of diatoms between cold and warm years against the 14-
267 year climatology. Zooplankton biomass for the Z1 and Z2 model classes were depth-integrated
268 over the 0-100 m depth range. However, because the model allows for more variability in the
269 grazing parameter than it does for zooplankton biomass, we focused on the proportion of depth-
270 integrated zooplankton grazing on diatoms and nanoflagellates over the same depth range
271 (0–100 m), as opposed to biomass per se.
272
273 2.6 Model Experiments
274 We performed a series of ten model experiments to determine the mechanistic links
275 between NPGO and the environmental parameters responsible for changes to phytoplankton in

the Central SoG (Table 1). First, we selected 2008 as a "typical" cold year (CY) and 2019 as a "typical" warm year (WY) from the four strongest NPGO positive and negative years, respectively. We then independently tested each of the environmental parameters of interest by applying individual parameters from a given CY to the original WY and vice versa. Five parameters were selected for the experiments: domain-wide winter nutrient concentration, diatom temperature response, winds, atmospheric thermal and radiative forcing, and river flow. For the nutrient experiments, initial (beginning January 1) nitrate and silicon concentrations were traded between CY and WY simulations. The temperature response experiments involved increasing the optimum temperature threshold for diatom growth from 12ºC to 15ºC in both CY and WY runs. The wind experiments traded CY and WY HRDPS winds throughout the year. The atmospheric thermal and radiative forcing experiments (hereafter thermal forcing) included changing the atmospheric components: incoming solar radiation, air temperature, long wave radiation, precipitation, and humidity throughout the year. Lastly, the river experiments involved switching the annual river flow into the Salish Sea from a given WY/CY to the experimental CY/WY. Model experiments were run for the entire year beginning January 1 and results were compared to the original CY/WY run.

2.7 Limitations of Diatom: Nanoflagellate Growth

Theoretical surface (0.5 m) diatom to nanoflagellate growth ratios were calculated as a function of temperature dependence only, nutrient dependence only, and the combined effect of temperature dependence, nutrient dependence, and maximum growth rate on phytoplankton growth. Monthly seasonal values are presented for the original cold (2008) and warm (2019) years, as well as for each of the model experiments. Theoretical diatom to nanoflagellate growth

299 ratios >1 are indicative of diatom-favoured growth whereas values <1 indicate nanoflagellate-
300 favoured growth.

301
302
303 **Table 1.** Model experiments used to determine the mechanistic link between NPGO and the
304 environmental parameters responsible for changes to phytoplankton in the Central SoG.
305 Parameters from the experimental warm year (WY) and cold year (CY) were applied to the
306 original CY and WY, respectively. Thermal includes atmospheric components, incoming solar
307 radiation, air temperature, long wave radiation, precipitation, and humidity.
308
309
310

Parameter	Experiment
Nutrients	1. WY with initial (January 1) CY nitrate and silicon 2. CY with initial (January 1) WY nitrate and silicon
Temperature Threshold	3. WY with diatom temperature threshold increased from 12ºC to 15ºC 4. CY with diatom temperature threshold increased from 12ºC to 15ºC
Winds	5. WY with CY winds 6. CY with WY winds
Thermal	7. WY with CY thermal 8. CY with WY thermal
Rivers	9. WY with CY rivers 10. CY with WY rivers

311

312

313 **3 Results**

314 3.1 NPGO Index

315 During the 14-year time series analyzed in this study, the annual NPGO index was in the
316 positive ("cool") phase from the end of 2007 to 2013 (Fig. 2). Monthly NPGO index values
317 showed a shift to the negative phase in October 2013 (Supp. Fig. S2). The annual NPGO
318 negative (warm) phase persisted from 2014 to the end of the study period in 2020 (Figs. 2, S2).
319 We note that this gives us only one phase change over the time series and our analysis is
320 cognizant of this limitation.

321

322 3.2 Physical Drivers

323 Mean monthly sea surface temperatures (SST) in the Central SoG averaged as a
324 climatology over the four coldest and four warmest years indicated that spring and mid-summer
325 SST (April to July) was higher during warm years with a maximum of 19.1 and 20.1°C for cold
326 and warm years, respectively (Fig. 3a). In contrast, SST was similar between cold and warm
327 years during autumn and winter (October to March). A comparison of mean seasonal SST
328 revealed a statistically significant difference in SST between cold and warm years in spring
329 (March to May; t-test, $t(3) = -3.85$, $p = 0.01$), but not summer (June to August; t-test, $t(3) =$
330 -2.20, $p = 0.07$; Fig. 3a).

331 Mean monthly sea surface salinity (SSS) during warm years was lower, i.e., fresher, than
332 cold years during the winter and spring months (November to May), but higher during the
333 summer and early fall months (June to October; Fig. 3b), largely driven by the high SSS values
334 observed in 2015 (Supp. Fig. S3). Similar to SST, a statistically significant difference in mean
335 seasonal SSS was observed for spring with a mean of 23.0 and 20.4 g/kg for cold and warm

336 years, respectively (t-test, $t(3) = –2.69$, $p = 0.04$), but not summer (t-test, $t(3) = –0.44$, $p = 0.68$;
337 Fig. 3b). Halocline strength, a proxy for stratification, was higher (stronger) in winter and spring
338 (November to May) during warm years compared to cold years (Fig. 3c), but similar during the
339 summer months (June to October) due to the relatively weak halocline values observed in
340 summer 2015 (Supp. Fig. S3). A statistically significant difference in mean seasonal halocline
341 strength was observed for spring with a mean of 1.04 and 1.57 g/kg m^{-1} for cold and warm years,
342 respectively (t-test, $t(3) = –3.25$, $p = 0.02$), but not for summer (t-test, $t(3) = 0.04$, $p = 0.97$; Fig.
343 3c).

344 Mean monthly surface PAR was higher from March to June of warm years compared to
345 cold years (Fig. 3d). Mean seasonal surface PAR was statistically significantly different in spring
346 with values of 55.7 and 66.9 uE/m^{-2}/s for cold and warm years, respectively (t-test, $t(3) = –4.64$,
347 $p < 0.01$). A statistically significant difference was not observed in summer (t-test, $t(3) = –0.08$, p
348 $= 0.94$; Fig. 3d). Mean monthly wind speed was consistently lower during warm years compared
349 to cold years (Fig. 3e). Statistically significant differences were observed for both spring (t-test,
350 $t(3) = 2.95$, $p = 0.04$). and summer (t-test, $t(3) = 7.60$, $p < 0.01$; Fig. 3e).

351 Daily Fraser River flow values were higher during the spring and early summer (April to
352 June) of warm years compared to cold years (Fig. 3f). In contrast, July and August Fraser River
353 flow values were higher during cold years. Mean seasonal values of Fraser River flow were
354 significantly different in spring with a mean spring flow value of 2653 m^3 s^{-1} occurring during
355 cold years and 3493 m^3 s^{-1} during warm years (t-test, $t(3) = –2.51$, $p = 0.01$). Conversely, mean
356 seasonal values of Fraser River flow during summer were significantly higher during cold years
357 (7019 m^3 s^{-1}) compared to warm years (4871 m^3 s^{-1}; t-test, $t(3) = 9.50$, $p < 0.001$).
358

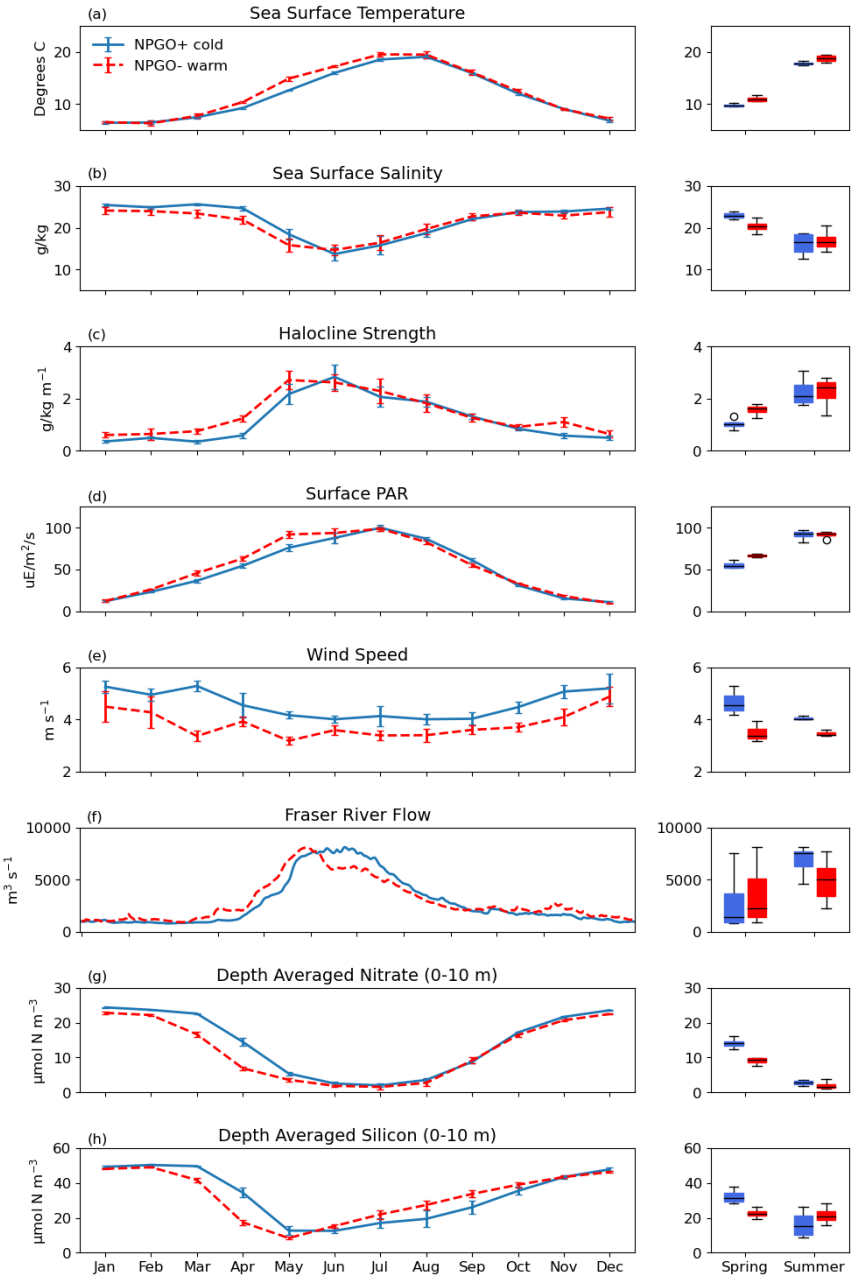

Figure 3. Mean monthly (left panels) and seasonal (right panels) values for local physical drivers and nutrient concentrations averaged over cold vs. warm years in the Central SoG, BC. Cold years are 2008, 2010, 2011, and 2012; warm years are 2015, 2018, 2019, and 2020. Daily values are provided for Fraser River flow.

369 3.3 Nutrients

370 Mean monthly seasonal cycles of 0-10 m depth-averaged nitrate concentrations were
371 lower during warm years compared to cold years throughout all months, with the most obvious
372 differences between warm and cold years occurring from March to May (Fig. 3g). A statistically
373 significant difference in mean seasonal nitrate concentrations was observed for spring with mean
374 nitrate concentrations of 14.2 and 9.04 μmol N m^{-3} for cold and warm years, respectively (t-test,
375 $t(3) = 5.61$, $p < 0.01$), but not for summer (t-test, $t(3) = 0.91$, $p = 0.40$). Like nitrate, lower silicon
376 concentrations were observed during warm years from January to May; however, silicon
377 concentrations during warm years were higher than those observed during cold years from June
378 through October (Fig. 3h). A statistically significant difference in mean seasonal silicon
379 concentrations was observed for spring with mean silicon concentrations of 32.3 and 22.5 μmol
380 N m^{-3} for cold and warm years, respectively (t-test, $t(3) = 3.68$, $p = 0.01$). No significant
381 difference was found between cold and warm years during summer (t-test, $t(3) = 1.06$, $p = 0.33$).
382 An analysis of nitrate and silicon concentrations along the thalweg (deepest connecting pathway
383 through the Salish Sea) indicated that higher nitrate and silicon concentrations at the outset of
384 NPGO positive (cold phase) years was prevalent throughout the Salish Sea (Supp. Fig. S5).
385
386 3.4 Phytoplankton Biomass
387 Mean monthly 0-100 m depth-integrated phytoplankton biomass began to increase in
388 April during cold years compared to an initial increase in biomass that occurred in March of
389 warm years (Fig. 4). The main peak in mean monthly diatom biomass occurred in May during
390 cold years (maximum of 32.9 mmol N m^{-2}; Fig. 4a) compared to an April peak of similar
391 magnitude in warm years (maximum of 31.2 mmol N m^{-2}; Fig. 4b). Following the main peak in

spring, diatom biomass was notably lower from June to September of the warm years compared to cold years. In addition, mean 0-100 m depth-integrated nanoflagellate biomass was higher from June to September of warm years compared to cold years, with a maximum nanoflagellate biomass of 32.8 mmol N m^{-2} in July; Fig. 4b). In contrast, the maximum flagellate biomass observed during cold years was only 22.7 mmol N m^{-2}.

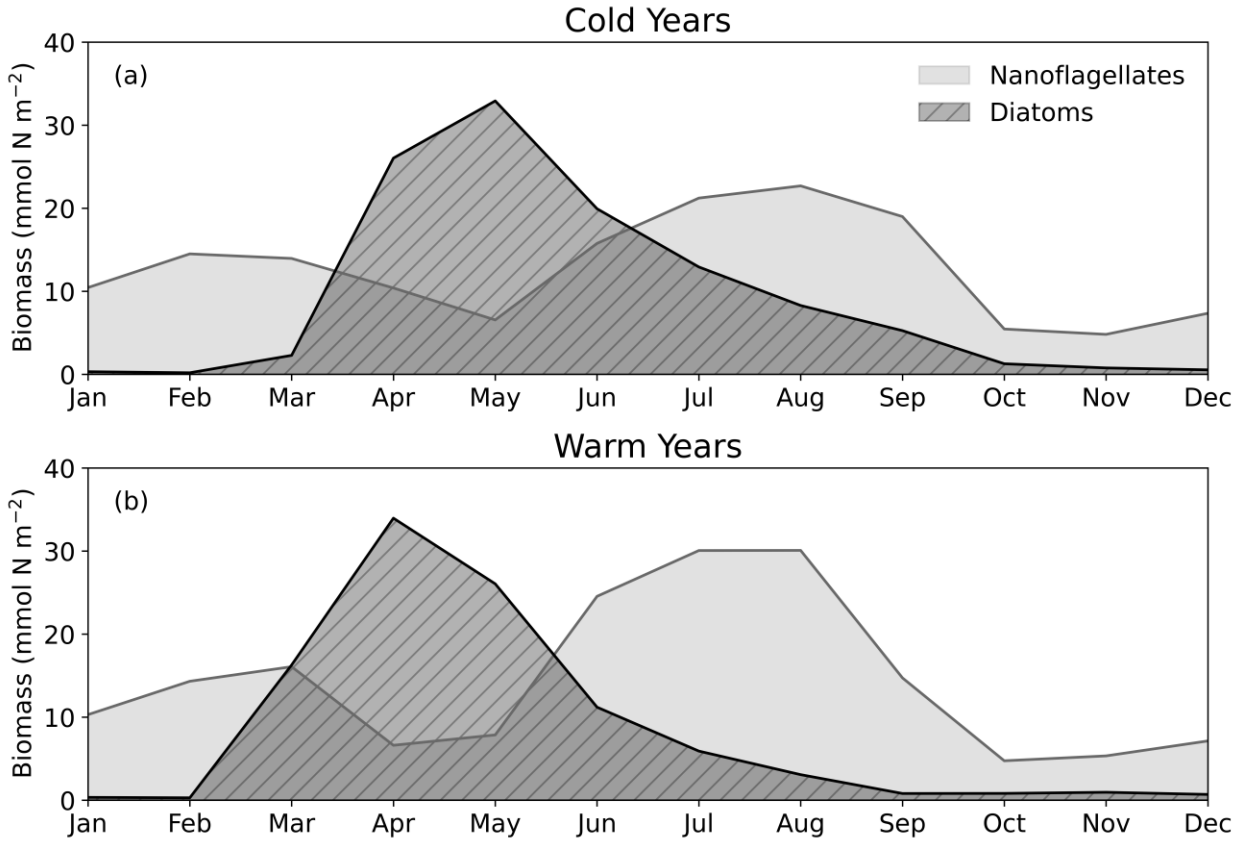

Figure 4. Mean monthly depth-integrated (0-100 m) diatom and nanoflagellate biomass averaged over (a) cold and (b) warm years in the Central Strait of Georgia, BC.

Temperature dependence and light/nutrient limitation on diatom growth showed that diatoms were more limited by temperature and nitrate in the surface waters during the summer

406 (July) of warm years compared to cold years in the Central SoG (Fig. 5). In contrast, diatoms in
407 the surface waters of the Central SoG were less limited by silicon during warm years, likely due
408 to the presence of fewer diatoms taking up silicon. Light limitation on diatom growth was similar
409 in the surface waters of cold and warm years (Fig. 5).

410

411
412

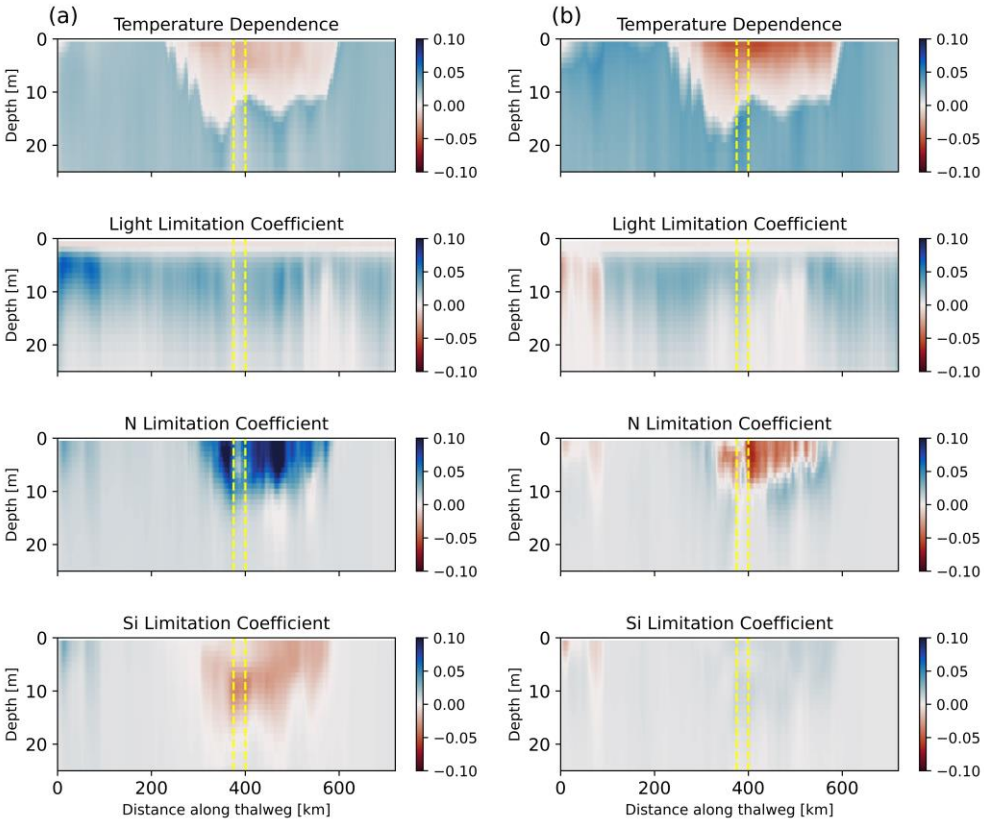

413

414 **Figure 5.** Diatom temperature dependence and anomalies in light and nutrient (nitrate, silicon)
415 limitation during (a) cold and (b) warm years compared to the 14-year climatology (2007-2020).
416 Yellow vertical lines indicate approximate bounds of our Central SoG region along the thalweg
417 (shown in Fig. 1). Colour bar is reversed so that blue = less limitation or temperature dependence
418 compared to climatology; red = more limitation or temperature dependence compared to
419 climatology. Data are from summer (July) 0-25 m; similar plots for spring are provided in Supp.
420 Fig S6).
421

422

3.5 Zooplankton grazing and biomass

Since the model allows for more variability in Z2 grazing than it does for biomass, we focused on the seasonal patterns of Z1 and Z2 grazing in warm-phase and cold-phase years (Fig. 6). Z1 grazed predominately on diatoms during April and May of cold years, but from March to May of warm years; however, maximum grazing rates were only slightly higher in cold years (5.3 μM N d^{-1}; May; Fig. 6a) compared to warm years (4.9 μM N d^{-1}; April; Fig. 6b). In contrast, the maximum Z2 grazing rates observed were higher in cold years (9.0 μM N d^{-1}; Fig. 6c) compared to warm years (7.4 μM N d^{-1}; Fig. 6d). During cold years, Z2 grazed predominately on diatoms from April to June compared to the March to May period of predominately diatom grazing observed during warm years. Most notably, both Z1 and Z2 exhibited substantial decreases in diatom grazing in June of warm years and a switch to higher flagellate grazing during the summer months (June to August), compared to cold years (Figs. 6b,d).

Due to the constraints on Z2 biomass in the model, we described differences in zooplankton biomass between cold and warm years for only the Z1 model class. Mean monthly depth-integrated Z1 biomass increased slightly earlier during warm years wherein maximum biomass occurred in April and remained high until September (Fig. 6b). Although Z1 biomass during cold years did not reach a maximum until July, the magnitude of the biomass peaks was similar at 1.5 g C m^{-2} d^{-1} and 1.7 g C m^{-2} d^{-1} for warm and cold years, respectively (Fig. 6a,b).

3.6 Model Experiments

3.6.1 Applying Cold Year parameters to Original Warm Year

The thermal and wind experiments had the strongest impacts on most parameters when experimental model runs using cold year (CY) parameters were compared to the original typical warm year (WY) (Fig. 7, Supp. Fig. S7). Applying the CY thermal forcing to the original WY resulted in lower SST during spring months whereas switching the winds from the CY to the WY lowered SST in July and August (Fig. 7a). The thermal experiment applied to the original WY, which included changing incoming solar radiation, was the only experiment to influence surface

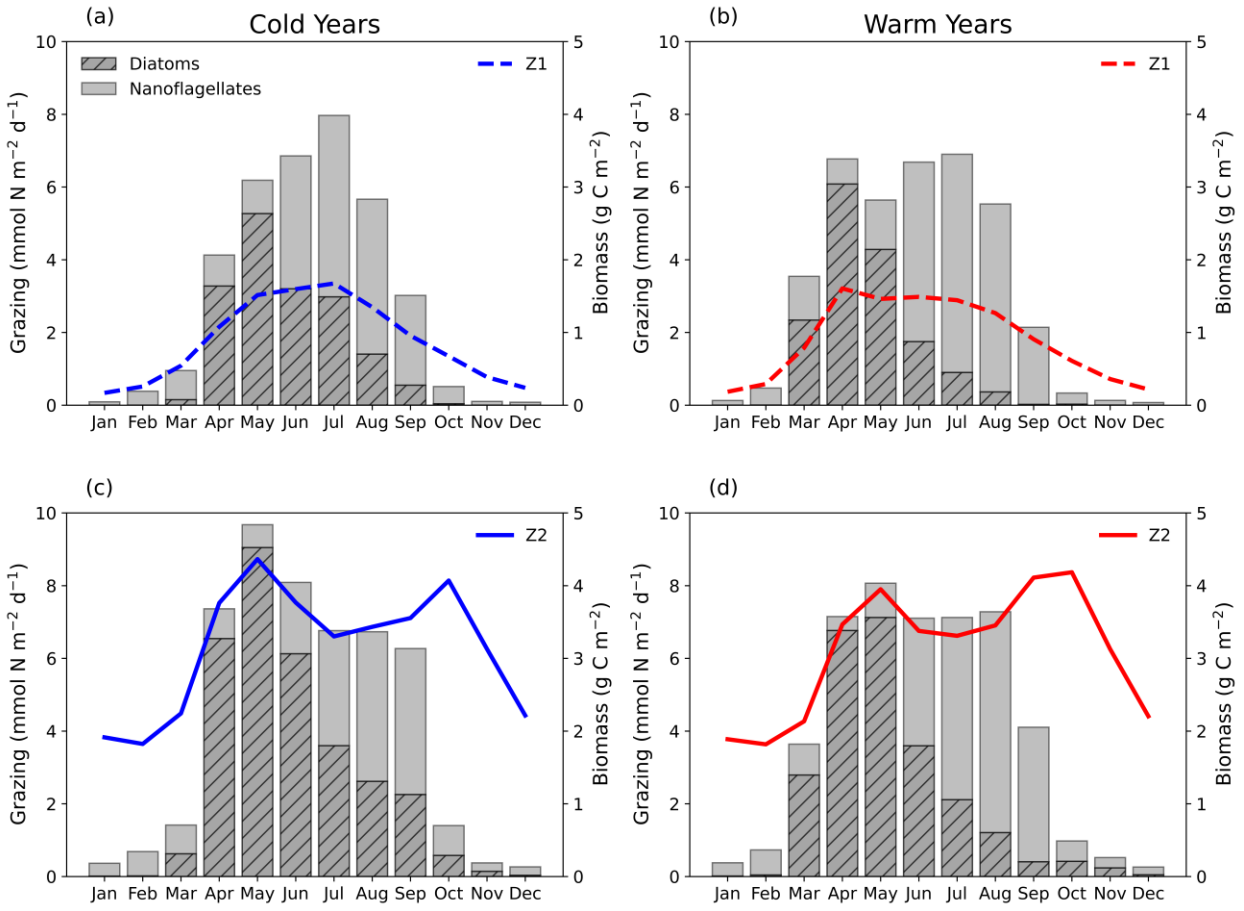

Figure 6. Depth-integrated (0-100 m) Z1 and Z2 grazing on diatoms and nanoflagellates (bars) and Z1 and Z2 biomass (lines) averaged over cold versus warm years in the Central SoG, BC.

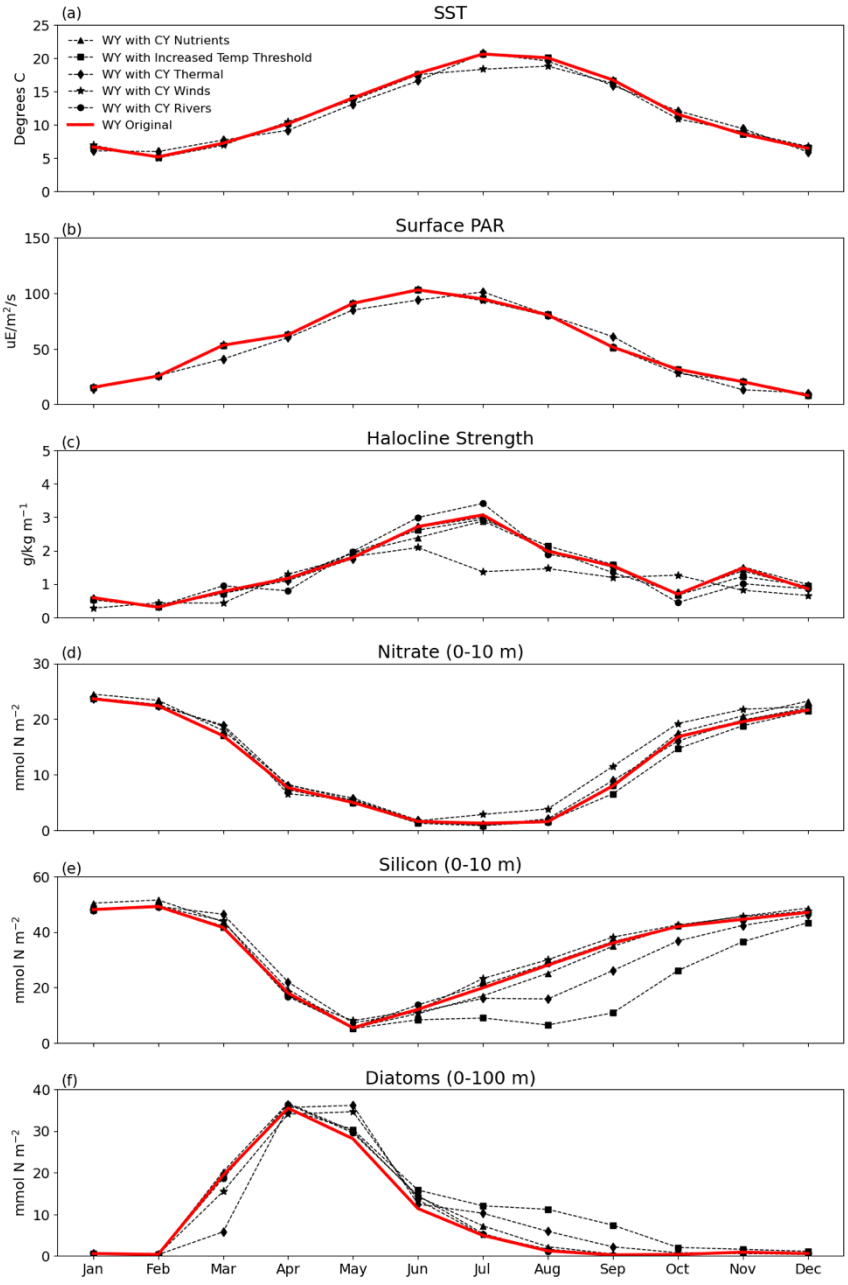

Figure 7. Results of model experiments taking a "typical" warm year (WY) and swapping parameters from a "typical" cold year (CY). Nitrate and silicon are depth-averaged over 0-10 m; diatoms are depth-integrated over 0-100 m.

PAR, decreasing PAR slightly from March to June compared to the original WY (Fig. 7b). Halocline strength was most strongly impacted by the wind experiment, which weakened the halocline during the summer months (June to August) when CY winds were applied to the WY (Fig. 7c). In addition, applying the CY rivers increased halocline strength during June and July.

Switching the initial nutrient conditions had little to no impact on the original WY, resulting in only a slight increase in 0-100 m depth-integrated diatom biomass from May to July (Fig. 7f). Yet, applying winds from the CY resulted in increases to both 0-10 m depth-averaged nitrate and silicon concentrations from July to September compared to the original WY (Figs. 7d,e). March diatom biomass decreased slightly when the CY winds were applied to the warm year, but there was a substantial decrease in March diatom biomass when the thermal conditions from the CY were applied to the WY (Fig. 7f). Conversely, CY thermal experiments resulted in an increase in diatom biomass from May through to September compared to the original WY; however, summer diatom biomass did not increase because of the CY winds. Overall, the experiment applying an increased temperature threshold for diatoms resulted in the largest increase in summer diatom biomass compared to the original WY (Fig. 7f). Both the thermal and threshold experiments resulted in a decrease in silicon concentrations from July through to November (Fig. 7e), likely due to higher diatom biomass taking up the silicon.

3.6.2 Applying Warm Year parameters to Original Cold Year

WY wind and thermal experiments also showed the strongest response when applied to the original CY (Fig. 8, Supp. Fig. S8). Applying the WY thermal forcing to the original CY resulted in an increase to spring (April to June) SST (Fig. 8a) and surface PAR (Fig. 8b), in addition to increase in March diatom biomass (Fig. 8f). The thermal experiment also slightly

490 decreased summer nitrate concentrations (Fig. 8d), which corresponded to a decrease in summer
491 diatom biomass (Fig. 8f) and an increase in summer silicon concentrations because of the
492 diatoms taking
493

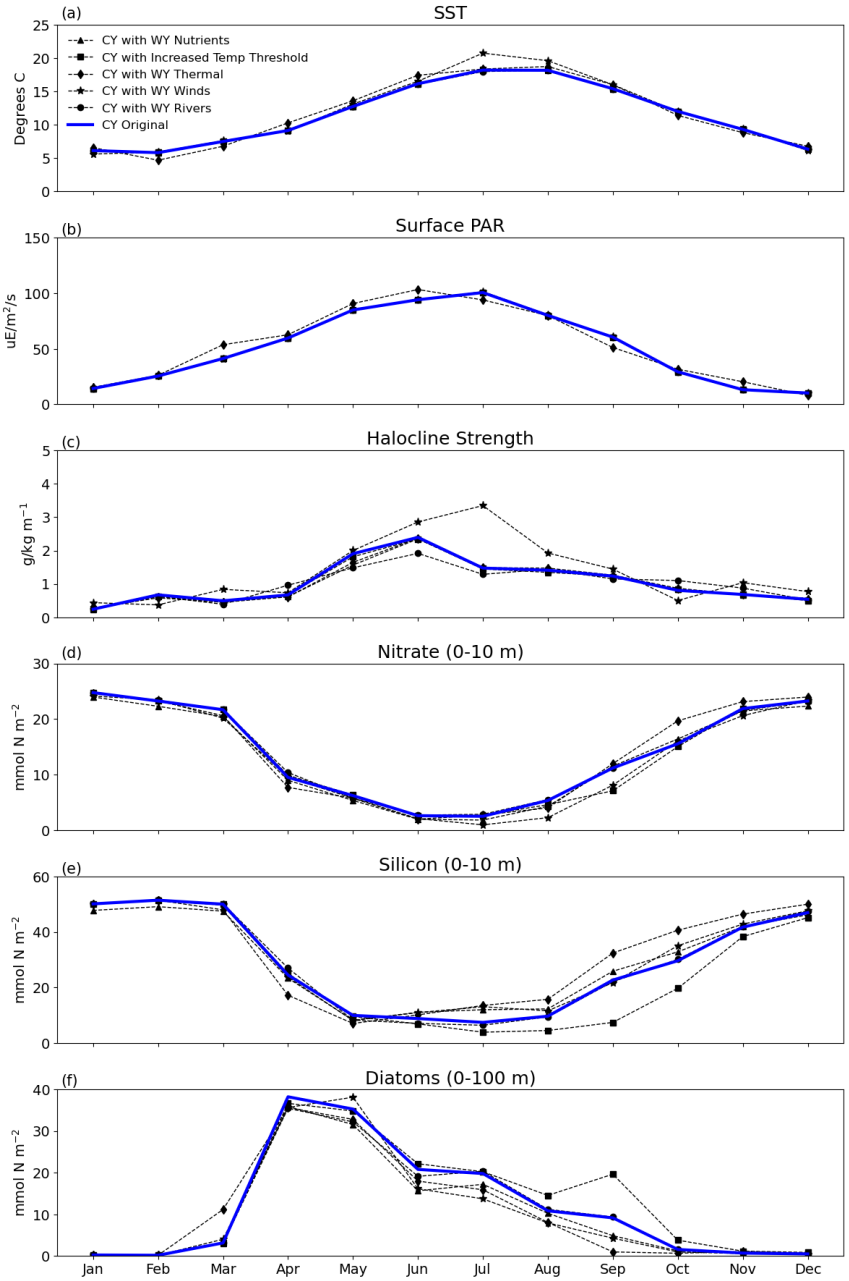

494
495
496 **Figure 8.** Results of experiments taking a "typical" cold year (CY) and swapping parameters
497 from a "typical" warm year (WY). Nitrate and silicon are depth-averaged over 0-10 m; diatoms
498 are depth-integrated over 0-100 m.
499

up less silicon (Fig. 8e). WY winds increased July SST (Fig. 8a) as well as halocline strength in March, and from June to August (Fig. 8c). In addition, WY winds decreased nitrate concentrations from May to September (Fig. 8d), but the wind experiment had little effect on silicon concentrations (Fig. 8e). Both WY wind and thermal applied to the CY decreased diatom biomass from May to September, but concentrations were not as low as those observed during the original WY (Fig. 8f). Applying the WY rivers to the CY resulted in an increase in halocline strength in April, but a weakening of the halocline between May and July (Fig. 8c). As a result, diatom biomass during the river experiments was lower from April to June when WY rivers were applied to the original CY (Fig. 8f). As was observed in the experiments with the original WY, increasing the temperature threshold for diatoms resulted in an increase in diatom biomass in August and September compared to the original CY (Fig. 8f).

3.7 Limitations on Diatom: Nanoflagellate Growth

We compared the theoretical ratio of diatom to nanoflagellate growth at the surface (0.5 m) between the original cold and warm year (2008 and 2019, respectively). These results were presented first to represent the general pattern observed for cold and warm years and were then compared to the results from the model experiments. They also demonstrated the extent to which the model temperature dependence stems directly from the chosen temperature-dependent rate parameterizations versus arising from a more complex interplay between model physics and nutrient supply; both effects are present in the model results. Temperature dependence on diatom:nanoflagellate growth was similar from October to April of the original warm (red line) and cold (blue line) years (Fig. 9a,d). The temperature

dependence of diatom:nanoflagellate growth decreased more rapidly in May of warm years. Diatom:nanoflagellate growth reached lower values, overall, during warm years with a minimum value of 1.38 in July. Similarly, nutrient limitation decreased diatom:nanoflagellate growth earlier during warm years with a substantial difference between warm and cold years being observed at the beginning in April (Fig. 9b,e). Diatom:nanoflagellate growth during warm years remained lower than values observed during cold years until August. When both temperature and nutrients were considered together, diatom:nanoflagellate growth decreased to values < 1 (i.e., nanoflagellate-favoured growth) from June to August of warm years (Fig. 9c,f). However, this ratio remained > 1 (i.e., diatom-favoured growth) during cold years. Thus, the model diatom:nanoflagellate response in warm versus cold years is driven by a combination of temperature and nutrient control.

Results from the model experiments showed that changing the initial nutrient conditions had virtually no impact on the WY nutrient and temperature dependence on diatom:nanoflagellate growth at the surface (Fig. 9; right panels) even though diatom biomass increased slightly (Fig. 7f). In comparison, applying the initial warm year nutrient conditions to the CY resulted in the diatoms:nanoflagellate showing a slight change towards nanoflagellate-favoured growth in July (Fig. 9c). Diatom:nanoflagellate growth increased in terms of temperature dependence for both experiments involving an increased temperature threshold for diatoms (Fig. 9a,d). Increasing the temperature threshold also impacted the nutrient dependence on diatom:nanoflagellate growth, which was lower due to the fact that more diatoms were taking up nitrate and silicon during the WY and CY of these experimental runs.

Overall, changing the winds has the most significant impact on the temperature and nutrient dependence of diatom and nanoflagellate growth. Our results showed that applying WY winds to a cold year brought the CY July and August diatom:nanoflagellate ratios <1.0 (nanoflagellate-favoured growth; Fig. 9c). Conversely, applying the CY winds to the warm

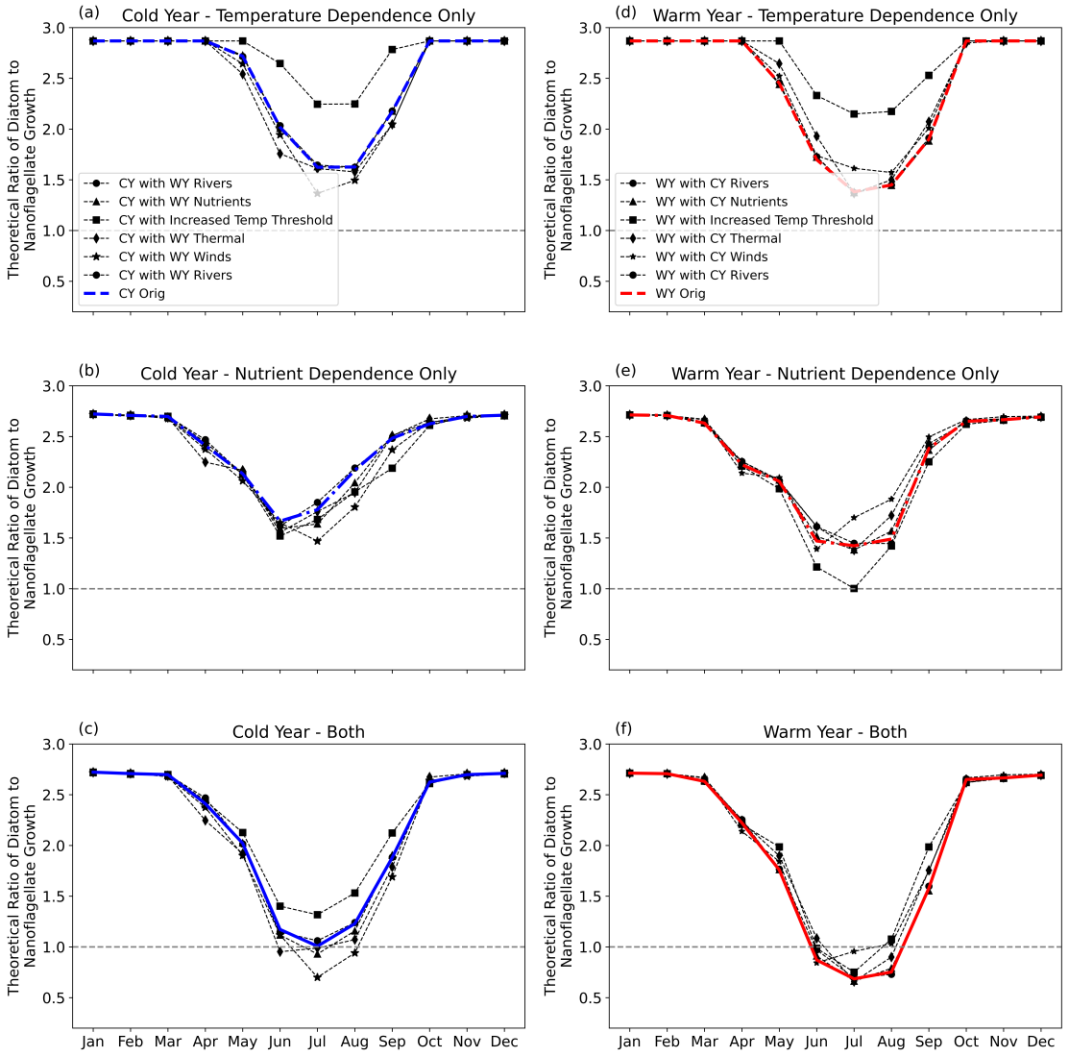

Figure 9. Theoretical diatom to nanoflagellate growth ratios at the surface (0.5 m) when temperature (a,d) and nutrient (b,e) responses are considered in isolation and then together (c,f). Values are multiplied by growth constants, which determine, but are not equal to, maximum growth rates in the model as the maxima of the temperature and nutrient response functions are not equal to one.

year resulted in an increase in diatom:nanoflagellate growth during July and August of the WY to ~1.0 (Fig. 9f). Changing the thermal forcing also impacted both the temperature and nutrient dependence of diatom and nanoflagellate growth, particularly in May and June, but not as severely as the winds (Fig. 9).

4 Discussion

4.1 Spring Phytoplankton Biomass

Our model results showed that spring diatom biomass increased earlier during NPGO negative (warm-phase) years in the Central SoG, which is consistent with previous satellite-based studies in the region (Suchy et al., 2019; Suchy et al., 2022). Earlier blooms can occur due to a number of factors including higher spring SST, increased freshwater runoff, increased stratification, more light (PAR), weaker winds, or a combination of these factors. The model experiments determined that thermal forcing had the strongest influence on spring diatom bloom timing in the Central SoG, followed by winds (but to a lesser degree). Although derived from different methods and a slightly larger study area, Suchy et al., (2022) also correlated the spring bloom in the Central SoG with both the NPGO and SST (and to PAR and wind). In contrast to our results, a 1-D model at a single location in the Central SoG found no direct relationship between temperature and spring bloom timing; however, a weak relationship was observed between bloom timing and NPGO ($r = 0.36$, $p = 0.05$; Allen & Wolfe, 2013), which supports our findings. Furthermore, Allen & Wolfe, (2013) showed that the occurrence of earlier than average spring blooms was strongly linked to weaker winds and decreased cloud cover, both of which result in an increase in SST. Warm-phase conditions can have both direct and indirect effects on phytoplankton, which is why the spring bloom is often correlated with numerous environmental

drivers. For example, warmer SST can increase the photosynthetic rate of phytoplankton cells (Henson et al., 2006) or increase cell division (Hunter-Cevera et al., 2016), thus causing phytoplankton biomass to increase earlier than normal. Alternatively, warm conditions may increase spring stratification and indirectly cause an earlier bloom to occur (Chiba et al., 2008). It should be noted that our model experiments revealed that the largest changes in spring diatom biomass were related to changes in light availability (Fig. 7) as opposed to SST, alone, in agreement with Allen & Wolfe, (2013).

As a consequence of the spring diatom biomass peaking earlier, the model also showed that nutrients became more limiting to diatom growth earlier (beginning in April) in the spring of warm-phase years (solid red lines; Fig. 9). In comparison, temperature dependence on diatom growth remained consistent from January to April between cold and warm years. In fact, the direct effects of temperature on the growth of diatoms and nanoflagellates were not observed until May and June of warm and cold years, respectively (Fig. 9). Below, we discuss how the conditions set up during the spring (March to May), and the resulting early spring peak in diatom biomass during warm-phase years, have implications for nutrient limitation in the summer (June to August). In addition, we discuss our model results in the context of the known implications on the match-mismatch of peak phytoplankton biomass available as food for zooplankton predators in the region during warm-phase years (Suchy et al., 2022).

4.2 Summer Phytoplankton Biomass

Warm-phase years exhibited lower overall summer diatom biomass and an earlier shift to nanoflagellate dominance compared to cold-phase years. Specifically, nanoflagellates dominated the phytoplankton biomass in July of warm-phase years, but not until August of cold-phase years

(Fig. 4). Similar shifts in the phytoplankton community have been observed in other regions in response to large-scale climate indices. For example, the negative NPGO (warm) phase was previously linked to shifts from diatom- to dinoflagellate-dominated communities in the California Current System (Fischer et al., 2020). In addition, negative NPGO (and positive PDO) periods with low winds and warmer temperatures have been associated with an earlier shift to dinoflagellate-dominated phytoplankton communities in San Luis Obispo Bay, also within the California Current System (Barth et al., 2020). Although SalishSeaCast does not explicitly model dinoflagellates, we compared our results to these studies with the understanding that our nanoflagellate group possesses characteristics similar to dinoflagellates including being smaller in size, slower-growing, and more efficient at growing in low nutrient conditions and on regenerated nutrients.

Previous SalishSeaCast model results found that phytoplankton in the Central SoG typically transition to increased nanoflagellate biomass near the beginning of June, with nanoflagellates then continuing to exhibit high biomass throughout the summer (Jarníková et al., 2022). Although *in situ* phytoplankton community composition studies are lacking in the region, HPLC-based studies have similarly shown that diatom-dominated blooms occur in spring in the Northern SoG, but transition to flagellate-type groups such as prasinophytes and cryptophytes during the summer (but diatoms are still present; Del Bel Belluz et al., 2021). Our model results are also supported by observations from Nemcek et al., (2023) who found that large centric diatoms predominate in spring (April) and then smaller mixed nanoflagellates including prasinophytes, haptophytes, cryptophytes, and raphidophytes (represented by our nanoflagellate model class; Supp. Fig. S1) predominate starting in early June when nitrate concentrations become limiting (Nemcek et al., 2023). Here we showed that the earlier shift to nanoflagellate-

627 dominated phytoplankton biomass during warm years was related to the increased nitrogen
628 limitation experienced by diatoms (Figs. 5, 9). On a global scale, increased ocean warming has
629 been shown to result in more nutrient-depleted conditions in the surface ocean, favouring small
630 phytoplankton at the expense of diatoms (Bopp et al. 2005). Therefore, we expect that any
631 additional climate signals contributing to warmer conditions and earlier spring blooms (e.g., El
632 Niño events, climate-induced warming) will produce similar results as those observed during
633 NPGO negative (warm-phase) years.
634
635 4.3 Summer Nutrient Re-supply
636 One key feature of the NPGO is its association with higher nutrient concentrations along
637 the northeast Pacific boundary (Di Lorenzo et al., 2009) and in the subarctic North Pacific
638 (Yasunaka et al., 2016) during cold-phase years. The positive-phase of the NPGO (cold years)
639 has been associated with changes in horizontal advection in the eastern North Pacific, with
640 intense westerly winds forcing nutrient-rich water southward from the subarctic to midlatitudes
641 (Yasunaka et al., 2016). These wind-induced changes were shown to deepen the mixed layer and
642 result in enhanced entrainment of nutrients in the surface waters (Yasunaka et al., 2016). In the
643 Central SoG, positive 0-10 m nitrate anomalies also predominated from 2007 and 2013,
644 corresponding to the NPGO positive (cold-phase) years, whereas negative nitrate anomalies
645 persisted during warm-phase years (2014-2020; Supp Fig. S2). An analysis of nitrate and silicon
646 concentrations along the thalweg (deepest portion along a transect) revealed that this pattern of
647 higher nitrate and silicon concentrations during NPGO positive (cold-phase) years was prevalent
648 throughout the Salish Sea and not limited to our Central SoG study region (Supp. Fig. S5).

649 The large-scale, basin-wide processes contributing to differences in regional nutrient
650 concentrations during NPGO negative and positive years were beyond the scope of this study.
651 However, the model experiments showed that nutrient concentrations at the beginning of the year
652 (lower during warm-phase years) had little effect on Central SoG diatom biomass in the spring
653 and summer. Instead, variability in wind-driven resupply of nutrients to the surface waters during
654 the summer (July and August) between cold- and warm-phase years had the most significant
655 impact on summer diatom biomass. The overall differences observed in mean wind speed
656 between cold and warm years were larger than, or at least on the same order of magnitude as, the
657 difference between winter and summer winds within a given year (Fig. 3e), thereby representing
658 substantial differences in mixing and nutrient resupply. Previously, Moore-Maley & Allen,
659 (2022) determined that wind-driven upwelling during the summer months results in periodic
660 nutrient resupply to the surface waters in the SoG. In addition, wind events in the Northern SoG
661 have been shown to result in episodic diatom blooms during summer (Del Bel Belluz et al.,
662 2021). These upwelling events are critical for resupplying nitrate to the surface waters and tend
663 to favour the opportunist-type diatoms in the model over the slower-growing nanoflagellates
664 which tend to do better in low nitrate conditions (Jarníková et al., 2022).
665 Applying the warm year (weaker) winds to the cold year experiment resulted in a
666 stronger halocline, a decrease in surface nitrate and silicon concentrations, and, ultimately, a
667 reduction in diatom biomass (Fig. 8d-f). In contrast, although applying the cold year winds to the
668 original warm year resulted in a weaker halocline coupled with an increase in nutrient
669 concentrations (Fig. 7d,e), no subsequent increase in summer diatom biomass was observed (Fig.
670 7f). We suspect that the conditions set up during the spring of warm years resulted in diatoms
671 being under too much temperature dependence/nutrient limitation for their biomass to recover

even though the ratio of diatom to nanoflagellate growth increased (Fig. 9), thus resulting in the predominance of nanoflagellates throughout the warm year summers.

4.4 Zooplankton Grazing

Overall, the total amount of food available to zooplankton was similar between cold and warm years. Mean grazing on diatoms and nanoflagellates combined was 3.0 and 3.2 μm N d^{-1} for Z1 and 4.1 and 3.9 μm N d^{-1} for Z2 for cold and warm years, respectively. Our results showed some evidence of higher grazing, periodically, during warm years. For example, both Z1 and Z2 zooplankton classes grazed on more food in March of warm years. In addition, total grazing by the Z2 model class was higher during July and August of warm years. Nevertheless, zooplankton in the model grazed on a higher proportion of nanoflagellates during warm years compared to cold years despite a set feeding preference for diatoms (0.28) over nanoflagellates (0.10; Suchy et al., 2023). Following the initial increase in diatom biomass in the spring, the Z1 model class grazed predominately on diatoms in March of warm years, but diatom-dominated grazing did not occur until April of cold years (Fig. 6). The Z1 and Z2 model classes both exhibited a decrease in diatom grazing in June of cold and warm years; however, this decrease in diatom grazing was more substantial in warm years and a switch to higher nanoflagellate grazing was observed to occur throughout the summer months (June to August) following the same pattern as we observed for phytoplankton biomass (Fig. 4).

These findings have implications in terms of the quality of the diet available to zooplankton given that phytoplankton groups have differing nutritional content and essential fatty acid composition (Jónasdóttir et al., 2005). In general, a mixed diet of both diatoms and flagellates is thought to provide the necessary essential fatty acids for the growth and

development of zooplankton in the region (El-Sabaawi et al., 2009 and references therein). Therefore, our results suggest that the nanoflagellate-predominance during the summer months of warm-phase years, coupled with the low biomass of diatoms as a supplemental food source, may have resulted in a lower quality diet for zooplankton during strongly negative NPGO (warm-phase) years.

4.5 Implications for Higher Trophic Levels

In addition to the nutritional implications for zooplankton, the timing of the seasonal succession from a diatom- to nanoflagellate-dominated diet is important because these two phytoplankton groups represent different trophic pathways. Within the SoG, a phytoplankton community dominated by larger-celled diatoms (typical of spring) is thought to transfer energy more efficiently to higher trophic levels through the 'classic' food chain (Parsons et al., 1969; Harrison et al., 1983). Furthermore, a diatom-dominated phytoplankton community supports larger, lipid-rich copepods and euphausiids (Mackas et al., 2013; Suchy et al., 2022), which are high quality prey for juvenile fish. In comparison, a nanoflagellate-dominated phytoplankton community could shift the zooplankton community to smaller-sized individuals, which are of poorer quality to zooplanktivorous animals (Sommer & Lengfellner, 2008).

Mackas et al., (2013) determined that the SoG zooplankton biomass signal correlates positively with NPGO, negatively with temperature, and positively (but less consistently) with SoG salmon and herring anomalies; however, their study did not determine the proximal causal mechanisms of these relationships and only suggested that a potential timing match-mismatch within the SoG was involved. Furthermore, Perry et al., (2021) related zooplankton biomass anomalies and salmon marine survival to the warm-phase years of the PDO (corresponds to

718 negative NPGO) and spring bloom timing, but nutrient information and phytoplankton
719 community composition data were not included in their study. Since juvenile salmon typically
720 enter the SoG to feed anywhere from mid-April to late July, depending on the species, before
721 migrating to the open ocean (Beamish et al., 2010; Neville et al., 2015; Grant et al., 2017), we
722 examined our model results over this critical time period (Fig. 10c). Our results showed that
723 nutrient limitation changes the food quality for zooplankton during this critical period, from a
724 diatom- to nanoflagellate-dominated diet, during warm-phase years with earlier blooms. It is
725 possible that this poorer quality zooplankton diet during warm-phase years may be the link in the
726 previously observed relationships between zooplankton biomass anomalies and variations in
727 salmon survival in the region. We note that other climate signals (e.g., positive PDO phase, El
728

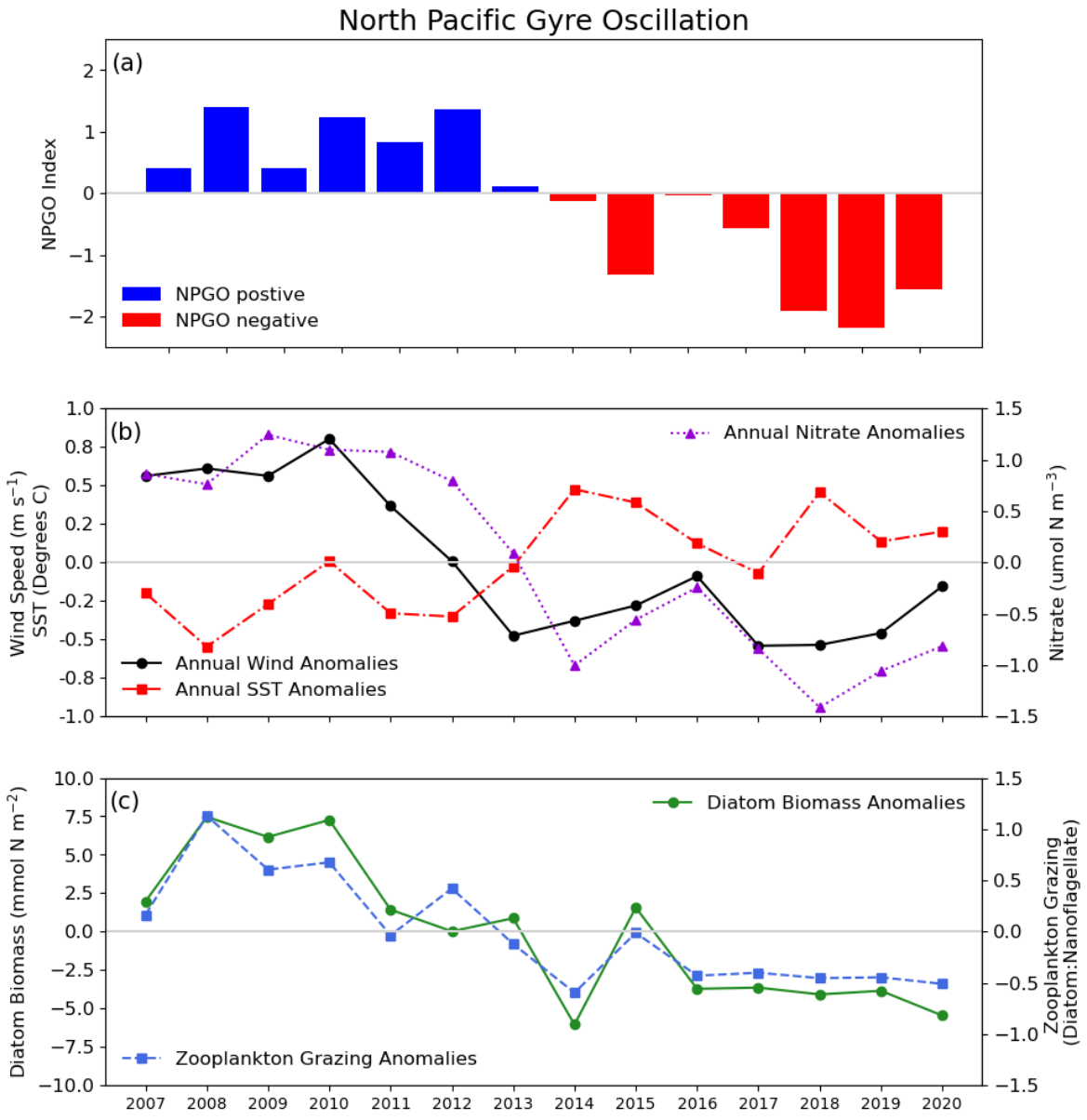

729

730 **Figure 10.** Summary Figure showing relationship between physical, chemical, and biological
731 anomalies in the Central SoG in relation to the NPGO index across SalishSeaCast model years
732 (a). Anomalies for HRDPS winds and model SST and 0-10 m nitrate (b) and anomalies in depth-
733 integrated (0-100 m) model diatom biomass and diatom:nanoflagellate grazing by zooplankton
734 averaged over the "critical period" for juvenile salmon (May to July).
735

736

737 Niño) and warming events (e.g., marine heatwaves) may also be associated with weaker winds,

738 increased SST, and increased stratification. Thus, in addition to the warm-phase of the NPGO,

we suspect that the quality of food for zooplankton may be affected by any warming scenario wherein a limited amount of nutrients are being resupplied to the surface waters in this region.

4.6 Study Limitations

We presented average cold vs. warm year results in this study for the sake of simplicity, but we note the importance of interannual variability in the Central SoG. Interannually, the environmental parameters showing the most consistent differences between our four cold and four warm years were SST, wind, and nitrate concentrations, particularly in the spring, while other parameters (e.g., halocline strength, Fraser River discharge) were more variable (Supps. Fig. S3). For example, 2015 was one of the warm-phase years, exhibiting the warmest SST, weakest winds, freshest water, and lowest nutrient concentrations during the spring months, which was a pattern that followed the other warm years in our study. However, winds during the summer of 2015 were more characteristic of the cold years in our study (i.e., stronger), resupplying enough nutrients to the surface waters to result in an increase in summer diatom biomass. In addition, Fraser River runoff during our "cold" year 2012 was exceptionally high in late spring/early summer compared to the other cold years. This high river flow co-occurred with weaker summer winds, which were more characteristic of warm years. As a result, we interpret our results with the understanding that other signals, i.e., marine heatwaves, El Niño, or La Niña events, are not mutually exclusive. Thus, the interannual variability in environmental parameters resulting from those signals may influence nutrient delivery to the surface waters, resulting in a pattern that diverges from our "average" conditions.

Furthermore, we note the importance of the spatial variability not considered in this study. Previous studies have highlighted distinct spatial patterns in the relationships between

762 climate variability and diatom abundance in the North Atlantic (Edwards et al., 2022). The
763 thalweg plots shown in Figure 5 indicate that the SoG is particularly impacted by both
764 temperature and nutrient limitation compared to other regions within the Salish Sea. Yet, even
765 within the SoG there exists spatial variability in how phytoplankton respond to different
766 environmental drivers (Suchy et al., 2019). Therefore, we highlight that our results are
767 representative of the Central SoG, only, and cannot necessarily be extrapolated to other
768 subregions of the Salish Sea given the distinct spatial and temporal variability present in other
769 regions (e.g., Jarníková et al., 2022; Suchy et al., 2023).
770
771 4.7 Model Limitations
772 Due to the optimum temperature imposed on diatom and nanoflagellate growth in the
773 model, we note that the model is likely overestimating the temperature effect we observed. The
774 combination of temperature and nutrient response employed in these simulations allowed the
775 model to successfully capture spring and summer nutrient and chlorophyll levels; however, it is
776 possible that a different set of parameters could represent the chlorophyll levels equally well, but
777 be better suited to the temperature and nutrient conditions in the Salish Sea. However, given the
778 good agreement overall, the over-estimation of the temperature effect must be compensated by
779 an underestimation of the nutrient effect in the model. That said, even after increasing the
780 model's optimum temperature for diatoms during the threshold experiments, cold year diatom
781 biomass was still higher compared to warm years. A sensitivity analysis across the full possible
782 temperature- and nutrient-response parameter space was outside the scope of this study.
783 Furthermore, although we can use the model to assess phytoplankton biomass and the
784 resulting food available to the Z1 and Z2 model classes, we were more restricted in our

conclusions about zooplankton biomass due to the imposed closure term of the Z2 zooplankton group. Drawing conclusions about the biomass of the Z2 class is complicated by the fact that the domain-wide biomass is set in the model. Thus, any changes that were observed in the Central SoG biomass reflects changes in the spatial pattern of Z2 throughout the entire model domain.

5 Conclusions

We used a three-dimensional coupled biophysical model, SalishSeaCast, to determine the mechanistic link between the NPGO and plankton dynamics in the Central SoG. The model showed that spring diatom biomass increased earlier during NPGO negative (warm-phase) years and that thermal conditions, followed by winds, had the strongest influence on bloom timing. NPGO negative (warm-phase) years exhibited lower overall summer diatom biomass and an earlier shift to nanoflagellate-dominance compared to NPGO positive (cold-phase) years because of conditions set up during the spring. This study revealed that variability in wind-driven resupply of nutrients to the surface waters during the summer (July and August) between cold- and warm-phase years had the most significant impact on summer diatom biomass, and ultimately on the food available to zooplankton grazers. As a result, the Z1 and Z2 model classes grazed on a higher proportion of nanoflagellates during the summer of warm-phase years, suggesting that zooplankton in warm years fed on a poorer quality diet during the critical period wherein juvenile salmon are feeding in the Central SoG.

Using the model experiments, our systematic analysis of the environmental drivers allowed us to isolate wind-driven resupply of nutrients during the summer as being the key determinant of variability in phytoplankton biomass in warm-phase versus cold-phase years. This mechanistic linkage is relevant in the context of any conditions (e.g., strong El Niño events,

positive phases of the PDO) favouring weaker winds or increased stratification, both of which limit the amount of nutrients being replenished to the surface waters. Ultimately, we may see an increase in the occurrence of nanoflagellate-dominated communities (Barth et al., 2020) as climate-change driven ocean warming continues.

Acknowledgments

This work was funded by the British Columbia Salmon Restoration and Innovation Fund of Fisheries and Oceans, Canada (grant #BCSRIF_2019_092). Computational resources for SalishSeaCast are provided by Compute Canada (now Digital Research Alliance of Canada), Ocean Networks Canada, and Advanced Research Computing and the Department of Earth, Ocean and Atmospheric Sciences both of the University of British Columbia. The SalishSeaCast model software environment was developed by Doug Latornell.

Open Research

SalishSeaCast model results (version 201905; Olson et al., 2020, Suchy et al., 2023) and model forcing fields are available online: (http://salishsea.eos.ubc.ca/erddap/griddap/index.html). The model code for NEMO-3.6 is available from the NEMO website (www.nemo-ocean.eu; Madec et al, 2017). Additional model runs for the model experiments will be available from the Canadian Federated Research Data Repository (Suchy et al, 2024a). The Jupyter Notebooks used for model output and analysis in this paper are available on GitHub preserved at https://zenodo.org/doi/10.5281/zenodo.10652235 (Suchy et al., 2024b)

Author Contributions

KDS performed the analyses and drafted the initial manuscript. SEA performed the hindcast simulations of SalishSeaCast and the model experiments. All authors contributed equally to the development of the research concept and to the manuscript beyond the initial draft.

References

Allen, S. E., & Wolfe, M. A. (2013), Hindcast of the timing of the spring phytoplankton bloom in the Strait of Georgia, 1968-2010, *Progress in Oceanography*, 115,6-13. doi:10.1016/j.pocean.2013.05.026

Barth, A., Walter, R. K., Robbins, I., & Pasulka, A. (2020), Seasonal and interannual variability of phytoplankton abundance and community composition on the Central Coast of California, *Marine Ecology Progress Series*, 637, 29-43. doi:0.3354/meps13245

Batten, S. D., Raitsos, D. E., Danielson, S., Hopcroft, R., Coyle, K., & McQuatters-Gollop, A. (2018), Interannual variability in lower trophic levels on the Alaskan Shelf, *Deep Sea Research Part II: Topical Studies in Oceanography*, 147, 58-68. doi:10.1016/j.dsr2.2017.04.023

Beamish, R. J., Sweeting, R. M., Lange, K. L., Noakes, D. J., Preikshot, D., & Neville, C. M. (2010), Early marine survival of Coho Salmon in the Strait of Georgia declines to very low levels, *Marine and Coastal Fisheries: Dynamics, Management, and Ecosystem Science*, 2(1), 424–39. doi:10.1016/j.pocean.2013.05.020

Beamish, R. J., Neville, C., Sweeting, R., & Lange, K. (2012), The synchronous failure of juvenile Pacific salmon and herring production in the Strait of Georgia in 2007 and the poor return of sockeye salmon to the Fraser River in 2009. *Marine and Coastal Fisheries: Dynamics, Management, and Ecosystem Science*, 4 (1), 403–414. doi:10.1080/19425120.2012.676607

Bond, N. A., Overland, J. E., Spillane, M., & Stabeno, P. J. (2003), Recent shifts in the state of the North Pacific, *Geophysical Research Letters*, 30(23), 2183, doi:10.1029/2003GL018597

Bond, N. A., Cronin, M. F., Freeland, H., & Mantua, N. (2015), Causes and impacts of the 2014 warm anomaly in the NE Pacific. *Geophysical Research Letters*. 42(9): 3414–3420. doi:10.1002/2015GL063306

Bopp, L., Aumont, O., Cadule, P., Alvain, S., & Gehlen, M. (2005), Response of diatoms distribution to global warming and potential implications: A global model study. *Geophysical Research Letters*, 32(19). doi:10.1029/2005GL023653

Chiba, S., Batten, S., Sasaoka, K., Sasai, Y., & Sugusaki, H. (2012), Influence of the Pacific Decadal Oscillation on phytoplankton phenology and community structure in the western North Pacific. *Geophysical Research Letters*, 39, L15603. doi:10.1029/2012GL052912

877 Davis, K. A., Banas, N. S., Giddings, S. N., Siedlecki SA, MacCready, P, Lessard, E. J., et al.
878 (2014), Estuary-enhanced upwelling of marine nutrients fuels coastal productivity in the
879 U.S. Pacific Northwest, *Journal of Geophysical Research: Oceans*, 119:8778-8799.
880 doi:10.1002/2014JC010248

881 Del Bel Belluz, J., Peña, M. A., Jackson, J. M., Nemcek, N. (2021), Phytoplankton composition
882 and environmental drivers in the northern Strait of Georgia (Salish Sea), British Columbia,
883 Canada, *Estuaries and Coasts*, 44:1419-1439. doi:10.1007/s12237-020-00858-2

884 Di Lorenzo, E., Schneider, N., Cobb, K. M., Franks, P. J. S., Chhak, K., Miller, A. J., et al.
885 (2008), North Pacific Gyre Oscillation links ocean climate and ecosystem change,
886 *Geophysical Research Letters*, 35, 1–6. doi:10.1029/2007GL032838

887 Edwards, M., Beaugrand, G., Kléparski, L., Hélaouët, P., & Reid, P. C. (2022), Climate
888 variability and multi-decadal diatom abundance in the Northeast Atlantic. *Communications*
889 *Earth & Environment*, 3(1), 162. doi:10.1038/s43247-022-00492-9

890 El-Sabaawi, R., Dower, J. F., Kainz, M., & Mazumder, A. (2009), Interannual variability in fatty
891 acid composition of the copepod *Neocalanus plumchrus* in the Strait of Georgia, British
892 Columbia, *Marine Ecology Progress Series*, 382,151-161. doi:10.3354/meps07915

893 Fischer, A. D., Hayashi, K., McGaraghan, A., & Kudela, R. M. (2020). Return of the "Age of
894 Dinoflagellates" in Monterey Bay: Drivers of Dinoflagellate Dominance Examined Using
895 Automated Imaging Flow Cytometry and Long-Term Time Series Analysis, *Limnology &*
896 *Oceanography*, 65, 2125–2141. doi:10.1002/lno.11443
897

Furey, N.B., Vincent, S.P., Hinch, S.G., & Welch, D.W. (2015), Variability in migration routes influences early marine survival of juvenile salmon smolts. *PLoS ONE*, 10 (10). doi:10.1371/journal.pone.0139269

Grant, S.C.H., Holt, C., Wade, J., Mimeault, C., Burgetz, I. J., Johnson, S., et al. (2018), Summary of Fraser River Sockeye Salmon (Oncorhynchus nerka) ecology to inform pathogen transfer risk assessments in the Discovery Islands, BC. *DFO Can. Sci. Advis. Sec. Res.*, Doc. 2017/074. v + 30 p.

Harrison, P. J., Fulton, J. D., Taylor, F. J. R., & Parsons, T. R. (1983), Review of the biological oceanography of the Strait of Georgia: Pelagic environment, *Canadian Journal of Fisheries and Aquatic Sciences*, 40:1064-1094. doi:10.1139/f83-12

Henson, S. A., Robinson, I., Allen, J. T., & Waniek, J. J. (2006), Effect of Meteorological Conditions on Interannual Variability in Timing and Magnitude of the Spring Bloom in the Irminger Basin, North Atlantic, *Deep-Sea Research I*, 53,1601-1615. doi: 10.1016/j.dsr.2006.07.009

Hertz, E., Trudel, M., Tucker, S., Beacham, T. D., Parken, C., Mackas, D., et al. (2016), Influences of ocean conditions and feeding ecology on the survival of juvenile Chinook Salmon (Oncorhynchus tshawytscha), *Fisheries Oceanography*, 25(4), 407-419. doi:10.1111/fog.12161

Hipfner, J. M., Galbraith, M., Bertram, D. F., & Green, D. J. (2020), Basin-scale oceanographic processes, zooplankton community structure, and diet and reproduction of a sentinel North

Pacific seabird over a 22-year period, *Progress in Oceanography*, 182, 102290. doi: 10.1016/j.pocean.2020.102290

Hunter-Cevera, K. R., Neubert, M. G., Olson, R. J., Solow, A. R., Shalapyonok, A., & Sosik, H. M. (2016), Physiological and ecological drivers of early spring blooms of a coastal phytoplankter, *Science*, 354, 326–329. doi: 10.1126/science.aaf8536

IOC; SCOR & IAPSO (2010) The international thermodynamic equation of seawater - 2010: Calculation and use of thermodynamic properties. Intergovernmental Oceanographic Commission, UNESCO (English), pp. 196pp.

Jarníková, T., Olson, E. M., Allen, S. E., Ianson, D., & Suchy, K. D. (2022) A clustering approach to determine biophysical provinces and physical drivers of productivity dynamics in a complex coastal sea, *Ocean Science*, 18,1451-1475. doi:10.5194/os-18-1451-2022

Jónasdóttir, S. H., Trung, N. H., Hansen, F., & Gärtner, S. (2005), Egg production and hatching success in the calanoid copepods Calanus helgolandicus and Calanus finmarchicus in the North Sea from March to September 2001, *Journal of Plankton Research*, 27(12), 1239-1259. doi:10.1093/plankt/fbi091

Khangaonkar, T., Sackmann, B., Long, W., Mohamedali, T., & Roberts, M. (2012), Simulation of annual biogeochemical cycles of nutrient balance, phytoplankton bloom(s), and DO in Puget Sound using an unstructured grid model, *Ocean Dynamics*, 62,1353-1379. doi: 10.1007/s10236-012-0562-4

940 Li, M., Gargett, A., Denman, K. (2000), What determines seasonal and interannual variability of
941 phytoplankton and zooplankton in strongly estuarine systems? application to the semi-
942 enclosed estuary of Strait of Georgia and Juan de Fuca Strait, *Estuarine, Coastal and Shelf*
943 *Science*, 50, 467–488. doi:10.1006/ecss.2000.0593

944 Li, L., Mackas, D. L., Hunt, B. P. V., Schweigert, J., Pakhomov, E. A., Perry, R. I., et al. (2013),
945 Zooplankton communities in the Strait of Georgia, British Columbia, track large-scale
946 climate forcing over the Pacific Ocean, *Progress in Oceanography*, 115,90-102.
947 doi:10.1016/j.pocean.2013.05.025

948 Litzow, M. A., Hunsicker, M. E., Bond, N. A., Burke, B. J., Cunningham, C. J., Gosselin, J. L.,
949 et al. (2020), The changing physical and ecological meanings of North Pacific Ocean
950 climate indices, *Proceedings of the National Academy of Sciences*, 117(14), 7665-7671.
951 doi:10.1073/pnas.192126611

952 Lu, Y., Li, J., Lei, J., & Hannah, C. (2017), Impacts of model resolution on simulation of meso-
953 scale eddies in the Northeast Pacific Ocean, *Satellite Oceanography and Meteorology*,
954 2(2), 328. doi:/10.18063/som.v2i2.328

955 Mackas, D. L., Galbraith, M. D., Faust, D., Masson, D., Young, K., Shaw, W., et al. (2013),
956 Zooplankton time series from the Strait of Georgia: Results from year-round sampling at
957 deep water locations, 1990-2010, *Progress in Oceanography*, 115,129-159.
958 doi:10.1016/j.pocean.2013.05.019

Madec, G., Bourdall-Badie, R., Bouttier, P. A., Bricaud, C., Bruciaferri, D., Calvert, D., et al. (2017), NEMO ocean engine. Notes du pole modélisation Linstitut Pierre-simon Laplace (IPSL). Revis. 8625 from SVN Repos

Milbrandt, J. A., Bélair, S., Faucher, M., Vallée, M., Carrera, M. L., & Glazer, A. (2016), The pan-Canadian high resolution (2.5 km) deterministic prediction system, *Weather and Forecasting*, 31(6), 1791-1816. doi:10.1175/WAF-D-16-0035.1

Moore-Maley, B., & Allen, S. E. (2022), Wind-driven upwelling and surface nutrient delivery in a semi-enclosed coastal sea, *Ocean Science*, 18,143-167. doi:10.5194/os-18-143-2022

Morrison, J., Foreman, M. G. G., Masson, D. (2012), A method for estimating monthly freshwater discharge affecting British Columbia coastal waters, *Atmosphere-Ocean*, 50(1), 1–8. doi:10.1080/07055900.2011.637667

Nemcek, N., Hennekes, M., Sastri, A., & Perry, R. I. (2023), Seasonal and spatial dynamics of the phytoplankton community in the Salish Sea, 2015-2019, *Progress in Oceanography*, 103108. doi:10.1016/j.pocean.2023.103108

Neville, C. M., Beamish, R. J., & Chittenden, C. M. (2015), Poor survival of acoustically tagged juvenile Chinook salmon in the Strait of Georgia, British Columbia, Canada, *Transactions of the American Fisheries Society*, 144 (1), 25–33. doi: 10.1080/00028487.2014.954053

Olson, E. M., Allen, S. E., Do, V., Dunphy, M., & Ianson, D. (2020), Assessment of nutrient supply by a tidal jet in the northern Strait of Georgia based on a biogeochemical model, *Journal of Geophysical Research: Oceans*, 125,1-25. doi:10.1029/2019JC015766

Parsons, T. R., Stronach, J., Borstad, G. A., Louttit, G., & Perry, R. I. (1981), Biological fronts in the Strait of Georgia, British Columbia, and their relation to recent measurements of primary productivity, *Marine Ecology Progress Series*, 6,237-242.

Pawlowicz, R., Riche, O., & Halverson, M. (2007), The circulation and residence time of the Strait of Georgia using a simple mixing-box approach, *Atmosphere-Ocean*, 45,173-193. doi:10.3137/ao.450401

Peña, M. A., Masson, D., & Callendar, W. (2016), Annual plankton dynamics in a coupled physical–biological model of the Strait of Georgia, British Columbia, *Progress in Oceanography*, 146,58-74. doi:10.1016/j.pocean.2016.06.002

Perry, R. I., Young, K., Galbraith, M. D., Chandler, P. C., Velez-Espino, A., & Baillie, S. (2021), Zooplankton variability in the Strait of Georgia, Canada, and relationships with marine survivals of Chinook and Coho salmon, *PLoS One*, 16(1),e0245941. doi:10.1371/journal.pone.0245941

Siedlecki, S. A., Banas, N. S., Davis, K. A., Giddings, S., Hickey, B. M., MacCready, P., et al. (2015), Seasonal and interannual oxygen variability on the Washington and Oregon continental shelves, *Journal of Geophysical Research: Oceans*, 120(2), 608-633. doi:10.1002/2014JC010254

Sommer, U., & Lengfellner, K. (2008), Climate change and the timing, magnitude, and composition of the phytoplankton spring bloom, *Global Change Biology*, 14(6), 1199-1208. doi:10.1111/j.1365-2486.2008.01571.x

1000 Soontiens, N., Allen, S. E., Latornell, D., Le Souëf, K., Machuca, I., Paquin, J. P., et al. (2016),
1001 Storm surges in the Strait of Georgia simulated with a regional model, *Atmosphere-Ocean*,
1002 54,1-21. doi:10.1080/07055900.2015.1108899

1003 Soontiens, N., & Allen, S. E. (2017), Modelling sensitivities to mixing and advection in a sill-
1004 basin estuarine system, *Ocean Modelling*, 112,17-32. doi:10.1016/j.ocemod.2017.02.008

1005 Suchy, K. D., Allen, S. E., & Olson, E. (2024a), SalishSeaCast monthly runs for model
1006 experiments, Federated Research Data Repository [Dataset], doi will be provided

1007 Suchy, K. D., Allen, S. E., & Olson, E. (2024b), SalishSeaCast/Suchyetal_NPGOpaper: Source
1008 code for: Mechanistic links between climatic forcing and model-based plankton dynamics
1009 in the Strait of Georgia, Canada, (v2024.02.12), Zenodo [Code],
1010 https://zenodo.org/doi/10.5281/zenodo.10652235

1011 Suchy, K. D., Le Baron, N., Hilborn, A., Perry, R. I., & Costa, M. (2019), Influence of
1012 environmental drivers on spatio-temporal dynamics of satellite-derived chlorophyll a in the
1013 Strait of Georgia, *Progress in Oceanography*, 176,102134.
1014 doi:10.1016/j.pocean.2019.102134

1015 Suchy, K. D., Young, K., Galbraith, M. D., Perry, R. I., & Costa, M. (2022), Match/mismatch
1016 between phytoplankton and crustacean zooplankton phenology in the Strait of Georgia,
1017 Canada, *Frontiers in Marine Science*, 759. doi:10.3389/fmars.2022.832684

1018 Suchy, K. D., Olson, E., Allen, S. E., Galbraith, M., Herrmann, B., Keister, J. E., et al. (2023),
1019 Seasonal and regional variability of model-based zooplankton biomass in the Salish Sea

and evaluation against observations, *Progress in Oceanography*, 219, 103171. doi:10.1016/j.pocean.2023.103171

Thomson, R.E. (1981) Oceanography of the British Columbia coast. Department of Fisheries and Oceans Sidney, BC.

Valencia, B., Landry, M. R., Décima, M., & Hannides, C. C. (2016), Environmental drivers of mesozooplankton biomass variability in the North Pacific Subtropical Gyre, *Journal of Geophysical Research: Biogeosciences*, 121(12), 3131-3143. doi:10.1002/2016JG003544

Yasunaka, S., Ono, T., Nojiri, Y., Whitney, F. A., Wada, C., Murata, A., et al. (2016), Long-term variability of surface nutrient concentrations in the North Pacific, *Geophysical Research Letters*, 43(7), 3389-3397. doi:10.1002/2016GL068097